Presented at 1978 Nuclear Science Symposium,
18-20 October 1978, Shoreham-Americana Hotel,
Washington, D. C. To be published in IEEE
Trans. Nucl. Sci.

BNL 25258

CONF-781033--29

AZIMUTHAL SPREAD OF THE AVALANCHE IN PROPORTIONAL CHAMBERS*

H. Okuno,† J. Fischer, V. Radeka, and A. H. Walenta

Brookhaven National Laboratory
Upton, New York 11973

October 1978

*This research was supported by the U. S. Department of Energy: Contract No. EY-76-C-02-0016.

†On leave from Institute for Nuclear Study, University of Tokyo, Tanashi, Tokyo, Japan.

DISCLAIMER

AZIMUTHAL SPREAD OF THE AVALANCHE IN PROPORTIONAL CHAMBERS*

H. Okuno,† J. Fischer, V. Radeka, and A. H. Walenta

Brookhaven National Laboratory
Upton, New York 11973

ABSTRACT

The angular distribution of the avalanche around the anode wire in the gas proportional counter is determined by measuring the distribution of positive ions arriving on cathode strips surrounding the anode wire for each single event. The shape and width of the distribution depend on such factors as the gas gain, the anode diameter, the counting gas and the primary ionization density. Effects of these factors are studied systematically, and their importance for practical counter applications is discussed.

Introduction

It has been shown[1] recently that the avalanche in a proportional counter is well localized on one side of the anode wire and that this localized avalanche induces asymmetric charges on electrodes surrounding the anode wire.[2,3] Many applications of this effect have been pointed out and tested with multiwire proportional chambers (MWPC) and multiwire drift chambers (MWDC) in order to improve the position readout of such detectors. The half-gap discrimination in MWPC for x-ray imaging reduced the parallax problem,[4] the right/left ambiguity in MWDC was solved by measuring induced signals on potential wires or cathodes[2,5] and, more generally, the azimuthal angle of the electron drift around the anode wire was determined by induced signals on a set of electrodes surrounding the anode wire[6,7], which made it possible to interpolate the position of low energy x-rays between two anode wires.[3,8,9]

Since the asymmetry of induced charges depends on the azimuthal spread of the avalanche, detailed information about the phenomena is highly desirable for the effective use of it.

Particle rate effects in recent and future applications of MWPC's and drift chambers, particularly with long drift spaces, become a problem due to the accumulation of positive ions in the chamber. This distorts the electric field and affects the electron drift properties and the gas multiplication properties. Reduction of these effects is possible in some cases and for this the avalanche spreading mechanism will be helpful.

In this paper, we present the measurements of the angular spread of the avalanche. The experimental results are then explained by taking into account the electron diffusion in the drift and avalanche process, the space charge effect and the uv-photon effect.

Apparatus and Measurements

The measurements were carried out with a cylindrical counter with a segmented cathode and grid wires shown in Fig. 1. The cathode is divided into 36 segments and the width of each segment is 2.54 mm covering an azimuthal angle of 10°. Grid wires are placed between the cathode strips 1.6 mm apart from the cathode surface. Collimated ^{55}Fe x-rays (5.9 keV) and ^{241}Am α-rays (5.5 MeV) are injected parallel to the anode wire at a radial distance of 10 mm from the anode wire.

Electrons from the primary ionization drift toward the anode wire and are multiplied in the strong field near the anode wire. Positive ions produced in the avalanche process drift from the anode wire toward the cathode strips through the grid wires. Since the diffusion coefficient of positive ions is much smaller than that of electrons, the angular distribution of positive ions is considered to be a magnified image of the angular distribution of the avalanche around the anode wire.

For the efficient detection of positive ions, the grid wires play the following roles: (1) to accelerate positive ions in the relatively strong field between the grid wires and cathode strips, which results in the fast rising induced signal on the cathode strips; (2) to reduce the early part of the induced signals which is due to the positive ion motion near the anode wire; and (3) to reduce the cross talk of induced signals between adjacent cathode strips.

For coarse measurements of angular distribution, cathode strips were connected in groups of three to give 12 channels for 360°. For measurements of narrow distributions, the 12 channels were connected to one cathode strip each. The angular resolution is somewhat larger than one strip width (about 20° FWHM). Each channel is connected to a charge sensitive preamplifier[10] with a decay time constant τ = 200 μsec. The typical operating conditions for ^{55}Fe x-rays, with Ar (90%) + CH_4 (10%), are an anode voltage V_A = 2 kV, grid voltage V_G = 0.5 kV, and a grounded cathode. Positive ions arrive at the grid wire 1.5 ms after the avalanche and the expected rise time of the cathode signal is 200 μs. Examples of the cathode signals are shown in Fig. 2, where τ = 200 μs and polarities of the signals are inverted by the preamplifier. In Fig. 2, (a) shows the signal on the cathode strip where the primary ionization has started and (b) the signal on the opposite cathode strip. Immediate signals which appear on both cathode strips correspond to the positive ion motion in the vicinity of the anode wire and the later signal is due to the positive ion motion between the grid and the cathode.

The amplitude of each positive ion signal was measured and displayed on a storage oscilloscope using a sequential readout circuit shown in Fig. 3. The desired information is the amplitude of the second signal in Fig. 2(a), which is the difference between the maximum and the base line. This function is realized after integration in the preamplifier, by a switched base line restorer comprised of capacitor C_b and the FET switch and by sampling. The width of the weighting function is controlled simply by the time interval between opening the restorer switch (cutting off the FET) and activating the sample-and-hold circuit. This operation is equivalent to single clipping by a delay line. It is obviously more

*This research was supported by the U. S. Department of Energy: Contract No. EY-76-C-02-0016.

†On leave from Institute for Nuclear Study, University of Tokyo, Tanashi, Tokyo, Japan.

practical for the long time intervals needed here of up to several hundred microseconds, and more convenient due to simple variation of the measurement time interval, when required. The control logic is started by the anode signal. The measurement time on the signals from the cathode strips is started by turning off the FET restorer switch at the time just before the second pulse in Fig. 2(a), and the signal is sampled at or near its maximum. By restricting the measurement time only to the rise time of this signal, the sensitivity to low frequency noise and microphonism is reduced.

Angular distributions of positive ions were measured by varying the anode voltage for various kinds of gas mixtures and anode wire diameters. Typical distributions are shown in Fig. 4, where each horizontal step corresponds to the azimuthal angle of 30°. The "avalanche size" Q is defined as a charge collected on the anode wire in 1 μs (the true avalanche charge is about 2 times larger). Figures (a), (b), and (c) show the results for ^{55}Fe x-rays in Ar (90%) + CH_4 (10%) for anode diameter of 25.4 μm. These results show that in this case the avalanche spread does not fluctuate event-by-event even at very high gas gain. In the proportional region ($Q \leq 2 \times 10^6 e$), the shape of the distribution is well approximated by a gaussian distribution and the FWHM is less than 100°. Raising the voltage, the avalanche starts to surround the anode wire.

The shape in the semi-proportional region depends strongly on the gas gain, the gas mixture, and the primary ionization density. For gas mixtures of Ar and molecular quenchers (CH_4, CO_2), an avalanche surrounds the anode almost uniformly at very high gas gain. However, in CH_4 and C_3H_8, the shape of the distribution looks like a parabola and does not surround the anode. For the electronegative gas mixture, Ar (69.3%) + Isobutane (30%) + Freon $13B_1$ (0.7%), the shape of the distribution is completely different depending on the type of the saturated signal. In the first amplitude saturating region, (signal type II in Ref. 1) the shape looks like a triangle and the avalanche is confined on one side of the anode wire. However, in the second amplitude saturating region, (signal type III) the distribution is unstable and almost uniform with small fluctuations.

Measurements have been performed with two different sources: α-rays from a ^{241}Am source and x-rays from a ^{55}Fe source. The α particles stop within the sensitive volume of the counter leaving a 2.1 cm long ionization track parallel to the anode wire for P-10. The total ionization in the sensitive volume corresponds to an energy loss of $\Delta E \approx 3$ MeV. The x-ray from the ^{55}Fe source leaves only one ionization cluster corresponding to an energy loss of 5.9 keV.

The two sources allow the observation of the avalanche under different conditions. In order to obtain the same total avalanche size Q for the ^{55}Fe, as for the ^{241}Am, a much higher gas gain is needed, while the resulting avalanche occupies only a small part $\Delta\ell$ of the anode wire, resulting in a much higher space charge per wire length. $\Delta\ell$ is mainly determined by the diffusion of the ionization drifting from the location of conversion to the anode. For typical conditions using Ar (90%) + CH_4 (10%), one obtains $\Delta\ell \approx 0.9$ mm FWHM. For the same Q, the space charge per anode length will be about a factor of 15 higher for the ^{55}Fe signal than for the ^{241}Am signal. For the same gas amplification factor, however, the ^{241}Am gives a higher space charge than the ^{55}Fe due to the higher number of ion pairs in the primary ionization per wire length. One obtains $Q_{prim}/\Delta\ell \approx 4.8 \cdot 10^4$ mm^{-1} for ^{241}Am compared to $Q_{prim}/\Delta\ell \approx 2.2 \cdot 10^2$ mm^{-1} for ^{55}Fe using $\Delta\ell = 0.9$ mm, which is the size of the ionization cluster when it arrives at the gas amplification zone.

The avalanche spread has been measured as a function of avalanche size for different concentrations of quencher (CH_4) in Ar (Fig. 5) and for magic gas (Fig. 6). Since an influence of the anode wire diameter is expected, the avalanche spread has been measured for two standard gases, Ar (90%) + CH_4 (10%) and 100% CH_4, and for wire diameters ranging from 12.7 μm to 127 μm (Fig. 7).

Avalanche Spreading Mechanism

A number of possible effects leading to the avalanche spread are considered:

1) diffusion of electrons
2) repulsion from space charge in the avalanche
3) uv-propagation
4) other processes related to the avalanche (diffusion of metastables, etc.).

The complexity of the avalanche development and the number of different processes contributing to its spread around the wire makes it difficult to obtain a complete mathematical description. Here we are mainly interested in a qualitative analysis which allows us to separate the effects 1)...4) to a certain extent. It is possible to determine their order of magnitude and to explain their dependence on counter parameters as well as on operating conditions.

A first classification of the effects can be obtained analyzing the spread as a function of the anode voltage for the two sources ^{55}Fe and ^{241}Am (Fig. 8).

The contribution from diffusion of the electrons drifting to the anode is expected to depend only on the relative voltage change which is small in the region where sufficient gas amplification can be obtained. All other effects depend on the avalanche size or gas amplification factor. Therefore, the almost constant value for the spread in the low voltage region is interpreted to be mostly diffusion. The avalanche-related effects will be classified as either depending on the total charge of the avalanche (space charge effect) or on the gas amplification factor, which can be understood to be related to the mean electron temperature in the avalanche and, therefore, to various excitation and ionization phenomena (e.g., emission and absorption of uv-quanta).

The effects of space charge and uv-propagation will be different for the two sources. ^{55}Fe shows effects of uv-propagation and other effects from excited atoms and molecules because of the relative high gas gain necessary. ^{241}Am shows strong space charge effects, even at a low gas gain, due to its high ionization density.

Diffusion

The diffusion considered here is the transversal diffusion of electrons drifting from their location of production (primary ionization) to the avalanche region, and also the diffusion of electrons produced in the avalanche on their way towards the anode. The whole process can be described in one step when the energy dependence of the elastic and the various inelastic cross sections are taken into account determining the mean

electron energy ε and consequently D/μ. The diffusion of the positive ions can be neglected since even at the high field in the avalanche region D/μ is small and close to the low field value given by the ambient temperature.

The transversal diffusion in a cylindrical field for a charge drifting in radial direction approaching the anode is expected to be different from the diffusion in a homogeneous field due to an increasing restoring force.

For the calculation we use a simplified picture. The observer sits in the center of the electron cloud and notices, while the whole system drifts to the anode, a time dependent heating of the electrons and an increasing restoring force perpendicular to the direction of motion. In this picture the field $\hat{E}$ at a distance χ from the center of the electron cloud is split into two components, E_r and E_χ, responsible for the drift of the whole cloud and for the restoring force, respectively, (Fig. 9). Under the assumption that the restoring field does not influence the mean electron energy ε, which is only determined by $E_r(r)$, the current $\vec{j}$ can be separated into independent components j_r, j_χ and j_z.

For the current in χ-direction, one obtains

$$j_\chi = -D \frac{\partial n}{\partial \chi} - n\mu E_\chi \quad , \qquad (1)$$

with D the diffusion coefficient and μ the mobility, which after the aforementioned approximation does not depend on E_χ but on E_r.

With

$$E_\chi = E_r \cdot \frac{\chi}{r} \quad , \qquad (2)$$

one obtains

$$j_\chi = -D \frac{\partial n}{\partial \chi} - n\mu E_r \frac{\chi}{r} \quad .$$

With

$$\operatorname{div} \vec{j} = -\frac{\partial n}{\partial t} \quad ,$$

one obtains the diffusion equation

$$D \frac{\partial n^2}{\partial \chi^2} + \frac{\mu E_r}{r} \frac{\partial}{\partial \chi} (n\chi) = \frac{\partial n}{\partial t} \quad . \qquad (3)$$

With $\omega_{rms} = \frac{\chi_{rms}}{r}$, one obtains the final result

$$\omega^2_{rms} = 2 \int_{r_a}^{r_o} \frac{D}{\mu} \frac{1}{E_r} \frac{1}{r^2} \, dr \quad , \qquad (4)$$

which gives the rms angular spread of an electron starting at r_o and arriving at the anode of radius r_a.

Unfortunately, $\varepsilon_k = e\, D/\mu$ is not known over the whole range of E occuring in a proportional counter. For CH_4, a measurement in Ref. 11 gives $\varepsilon_k(E)$ up to $\varepsilon_k \approx 2$ eV. For the different mixtures of Ar with CH_4, a "mean electron" model[12] has been used to calculate $\varepsilon_k(E)$, Fig. 10. For further calculation, Eq. (4) has been split into two parts

$$\omega^2_{rms} = 2 \int_{r_a}^{r_c} \frac{\varepsilon_k}{E_r} \frac{1}{r^2} \, dr + 2 \int_{r_c}^{r_o} \frac{\varepsilon_k}{E_r} \frac{1}{r^2} \, dr \quad , \qquad (5)$$

where r_c is determined to be the radius where under the given conditions $\varepsilon_k = 2$ eV. The dependence $\varepsilon_k(E)$ up to 2 eV can be very well approximated by

$$\varepsilon_k = \varepsilon_o \left(\frac{E}{E_o} \right)^m \quad . \qquad (6)$$

A similar dependence, but with different exponent m, is assumed for $\varepsilon_k > 2$ eV. Clearly, the real curve $\varepsilon_k(E)$ may continue above 2 eV with the same exponent, as for the smaller E, until the increase of inelastic cross sections reduces the slope gradually. Therefore, the exponent obtained for $\varepsilon_k > 2$ eV represents a mean value.

The measurement of the spread for ^{241}Am at low gas gain, which is considered to be only due to diffusion, (after correcting for $\omega_o \approx 20^\circ$ FWHM of inherent width of the measurement) is used to determine m as defined in Eq. (6). Figure 10 shows the expected result, that the slope for $\varepsilon_k > 2$ eV $m \approx 0.5$ is smaller than for $\varepsilon_k < 2$ eV ($m \approx 1$) due to the onset of the inelastic cross sections. In the highest field region ($r \leq 100\ \mu$) mean electron energies of the order of $\varepsilon \approx 1.5\ \varepsilon_k \approx 10$ eV are reached in agreement with the fact that in this region ionization takes place (threshold for ionization in Ar, $\varepsilon_{Ar} = 15.7$ eV and in CH_4, $\varepsilon_{CH_4} = 13.0$ eV).

The comparison of the measured values for various anode diameters, with the prediction of Eq. (5) using $\varepsilon_k(E)$ as determined above for CH_4 and for Ar (90%) + CH_4 (10%), shows satisfactory agreement (Fig. 11) with the ^{241}Am data. For the data obtained for ^{55}Fe, one obtains calculated values about $10^\circ \ldots 20^\circ$ smaller than the measured ones. A small contribution by avalanche-dependent effects such as space charge or uv-effects is to be expected since even the lowest gas gain permitting a measurement is far above the gas gain for the ^{241}Am measurement.

Processes Related to the Avalanche

The spread of the avalanche from the ^{241}Am increases considerably above the value for diffusion at a gas gain, where the spread for the ^{55}Fe is still close to the diffusion value (Fig. 8). Therefore, this effect is contributed to space charge effects.

The space charge effect becomes also apparent in Fig. 12 where the spread is shown as a function of the avalanche size Q (total charge). Here the values for the ^{241}Am data increases at much higher Q in agreement with the fact that the ionization of the α-particle along the wire results for a given Q in a smaller space charge per wire length.

The spread due to uv-emission and absorption or due to other effects relying on highly excited atoms and molecules therefore will be observed only at highest voltage in the ^{55}Fe measurements. Figure 13 shows the spread for ^{55}Fe and ^{241}Am at constant avalanche size as a function of the inverse CH_4 concentration $1/[CH_4]$. The values are corrected for diffusion by subtracting quadratically the low voltage value. The measured points for ^{55}Fe suggest a spread proportional to $1/[CH_4]$

in agreement with the hypothesis of uv-spread where the mean free path of uv-absorption will be proportional to $1/[CH_4]$. The values for ^{241}Am are close to zero and are constant within the error bars.

Extrapolating the dependence for the ^{55}Fe values to an infinite CH_4 concentration, one finds a value for the spread well above the value for ^{241}Am showing evidence that another effect, dependent on the gas amplification factor, contributes to the spread. It may be possible that impurities in the counting gas having a lower ionization potential than CH_4 contribute a uv-effect independent of the CH_4 concentration. Since our measurement includes the spread of the avalanche over a time period of the order of 100 μs, long-living, excited states also may produce a delayed uv-effect or may even diffuse around the wire and ionize by encounters of the second kind.

Magic Gas Mixture

Figure 6 shows the angular spread in the electronegative gas mixture, Ar (69.3%), Isobutane (30%), and Freon $13B_1$ (0.7%). For the anode with a diameter of d = 25.4 μm, the spread is almost constant between an avalanche size of 10^7 to 10^8 and shows an increase for $Q > 10^8 e$. Similar behavior is found for other wire diameters. In the region of small angular spread, the signals are amplitude-saturated. It has been found (Ref. 1) that the center of gravity of the avalanche in this operating mode (signal type II) moves away from the wire if the high voltage is increased, which may explain why the angular spread remains constant or even seems to decrease with increasing voltage.

Increasing the high voltage further, the angular spread increases eventually for all three wire diameters investigated. This operating mode gives signals of type III (Ref. 1). Here one observes, also apart from the increasing spread, a different shape of the angular distribution as mentioned earlier. For the small wire diameter, the spread is large enough to surround the wire completely, while for the thick wire only a fraction of the wire periphery is covered by the avalanche. An absorption length $\lambda \approx 10$ μm for the photons could explain this behavior, but it is also possible that a critical field strength has to be reached before an electron from a uv-ionization in the neighborhood of the avalanche can initiate a new avalanche strong enough to produce enough uv-quanta for further ionization. The latter possibility, in principle, represents a discharge similar to the Geiger mode which also has a well defined threshold.

Conclusions

Three main contributions to the angular spread of the avalanche around the wire could be separated. In the linear mode of operation, where the total charge produced in the avalanche is proportional to the total charge of the primary ionization, the spread around the wire is mostly due to diffusion. In the semiproportional mode of operation, different effects are found to contribute to the avalanche spread depending on the type of primary ionization. For dense primary ionization (α-particles) at higher gas gain, space charge effects spread the avalanche further. Only at high gas gain in the semiproportional region for primary ionization with low density, (x-rays in the keV range, minimum ionizing particles) spread due to uv-emission and absorption becomes the main source of avalanche spread.

The amount of spread of the avalanche around the anode wire can be controlled by the choice of gas and the anode wire diameter. To achieve a small spread will be useful in applications where the center of gravity of angular distribution is to be measured with high accuracy. A wide spread may be preferred in a drift chamber in order to collect the positive ions from the avalanche on special grid wires to reduce the space charge in the drift region. This is an important aspect for high rate applications.

Acknowledgements

The authors wish to thank Prof. E. Gatti, on leave from the University of Milano, for many useful discussions. His contribution to the calculation of the diffusion is greatly acknowledged. We also thank L. C. Rogers for the design and construction of the readout electronics.

References

1. J. Fischer, H. Okuno, and A. H. Walenta, Nucl. Instr. & Meth. 151 (1978) 451.
2. A. H. Walenta, Nucl. Instr. & Meth. 151 (1978) 461.
3. G. Charpak, G. Peterson, A. Policarpo, and F. Sauli, Nucl. Instr. & Meth. 148 (1978) 471.
4. C. J. Borkowski and M. K. Kopp, IEEE Trans. Nucl. Sci., NS-24 (1977) 287.
5. A. Breskin, G. Charpak, and F. Sauli, Nucl. Instr. & Meth. 151 (1978) 473.
6. J. Fischer, H. Okuno, and A. H. Walenta, IEEE Trans. Nucl. Sci., NS-25 (1978) 794.
7. G. Charpak, G. Peterson, A. Policarpo, and F. Sauli, IEEE Trans. Nucl. Sci., NS-25 (1978) 122.
8. T. J. Harris and E. Mathieson, Nucl. Instr. & Meth. 154 (1978) 183.
9. H. I. Kochelev and V. I. Telnov, Nucl. Instr. & Meth. 154 (1978) 407.
10. V. Radeka, IEEE Trans. Nucl. Sci., NS-21 (1974) 51.
11. L. W. Cochran and D. W. Forester, Phys. Rev. 126 (1962) 1785.
12. A. H. Walenta, "Driftkammern", GSI Bericht P3-74, Arbeitstagung über Detektoren, Darmstadt, July, 1973.

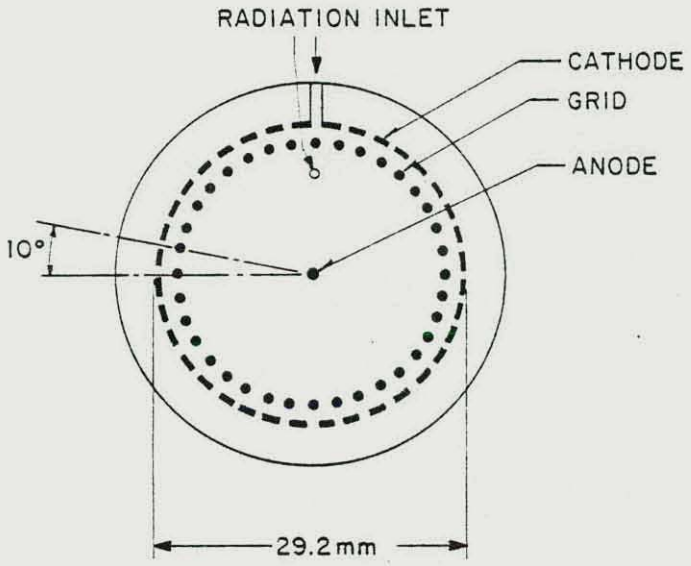

Fig. 1. The cylindrical counter with segmented cathode and grid wires.

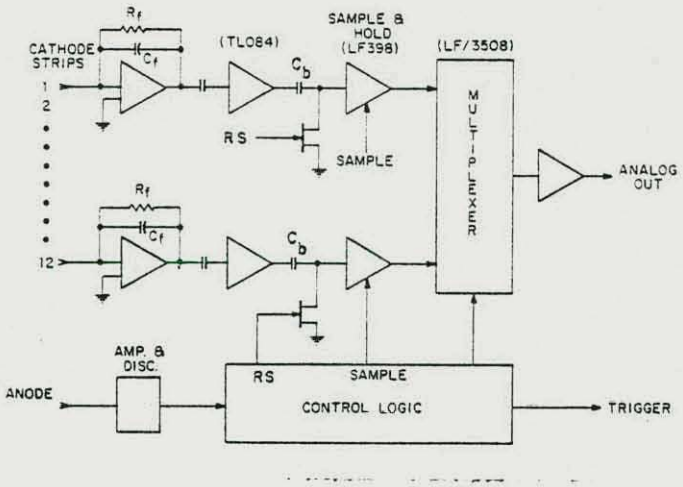

Fig. 3. Block diagram of the readout electronics. R_f = 100 MΩ, C_f = 2 pF. RS: restorer switch.

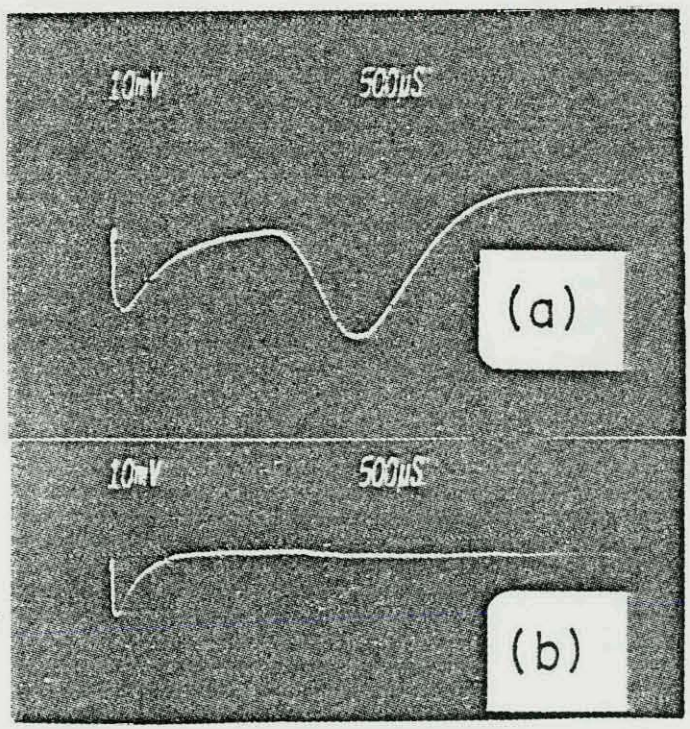

Fig. 2. Positive ion signals on cathode strips; (a) at the side or primary ionizations and (b) at the opposite side of primary ionizations for ^{55}Fe x-rays in Ar (90%) + CH_4 (10%). V_A = 2.0 kV, V_G = 0.5 kV, V_C = 0V and τ = 200 μs.

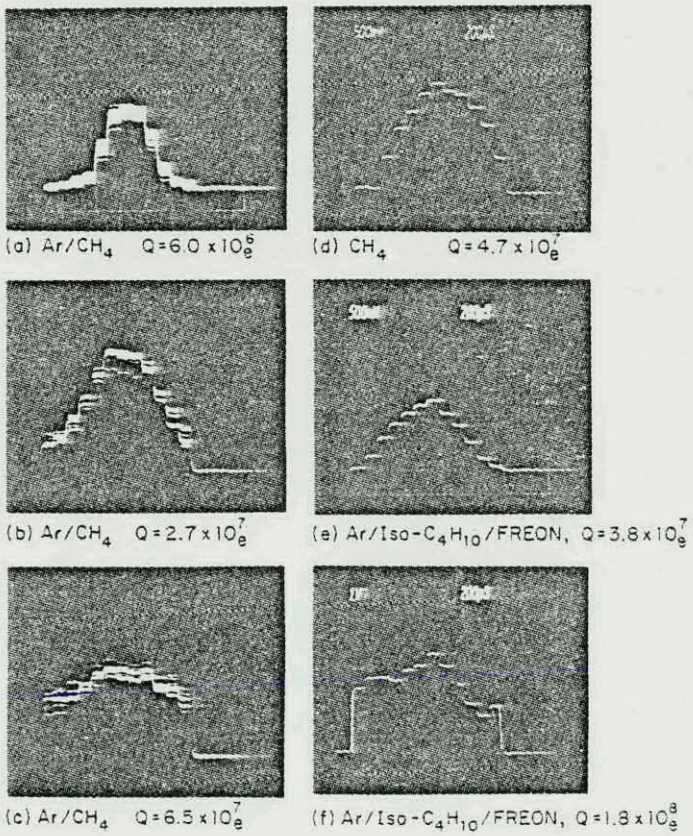

Fig. 4. Azimuthal angular distributions of the avalanche for ^{55}Fe x-rays with the anode of 25.4 μm in diameter. Q is the avalanche charge measured on the anode wire in 1 μs.

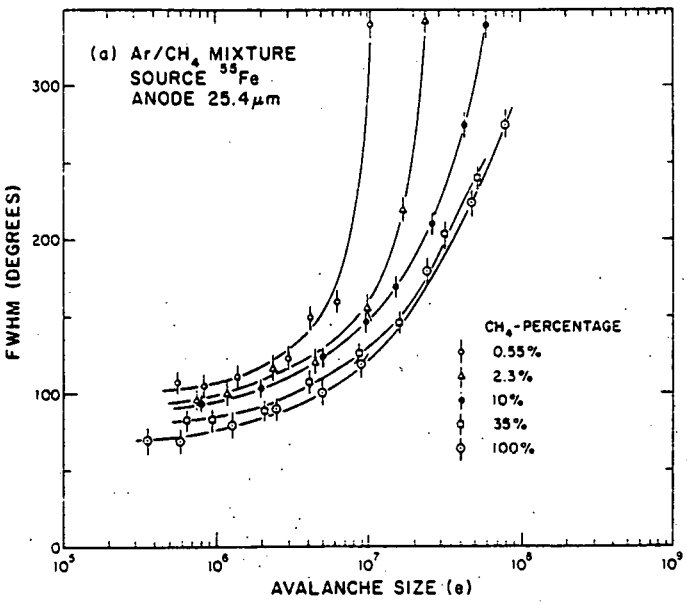

Fig. 5(a). FWHM of the angular distribution of the avalanche for ^{55}Fe x-rays in various Ar/CH_4 mixtures as a function of the avalanche size Q.

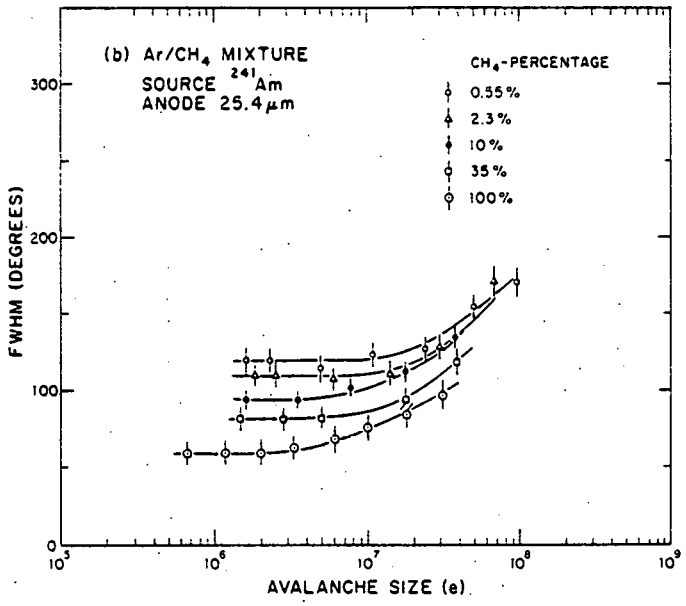

Fig. 5(b). FWHM of the angular distribution of the avalanche for ^{241}Am α-rays in various Ar/CH_4 mixtures as a function of the avalanche size Q.

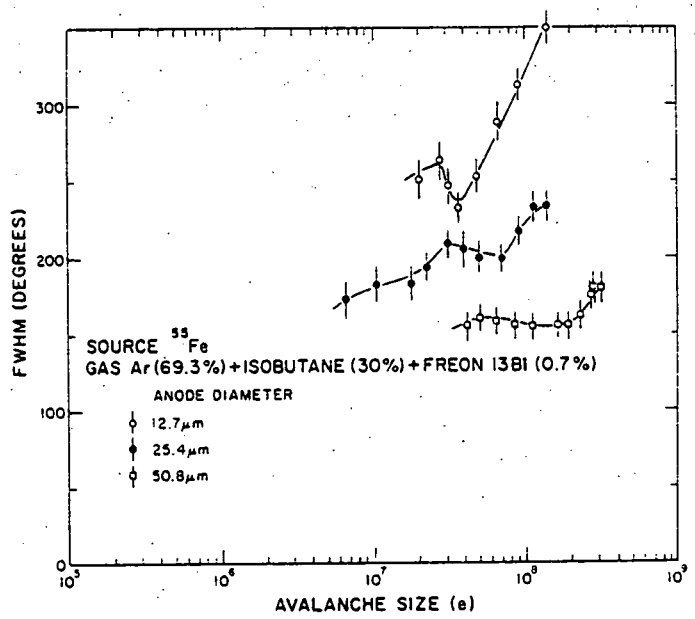

Fig. 6. FWHM of the angular distribution of the avalanche for ^{55}Fe x-rays in Ar (69.3%) + Isobutane (30%) + Freon $13B_1$ (0.7%).

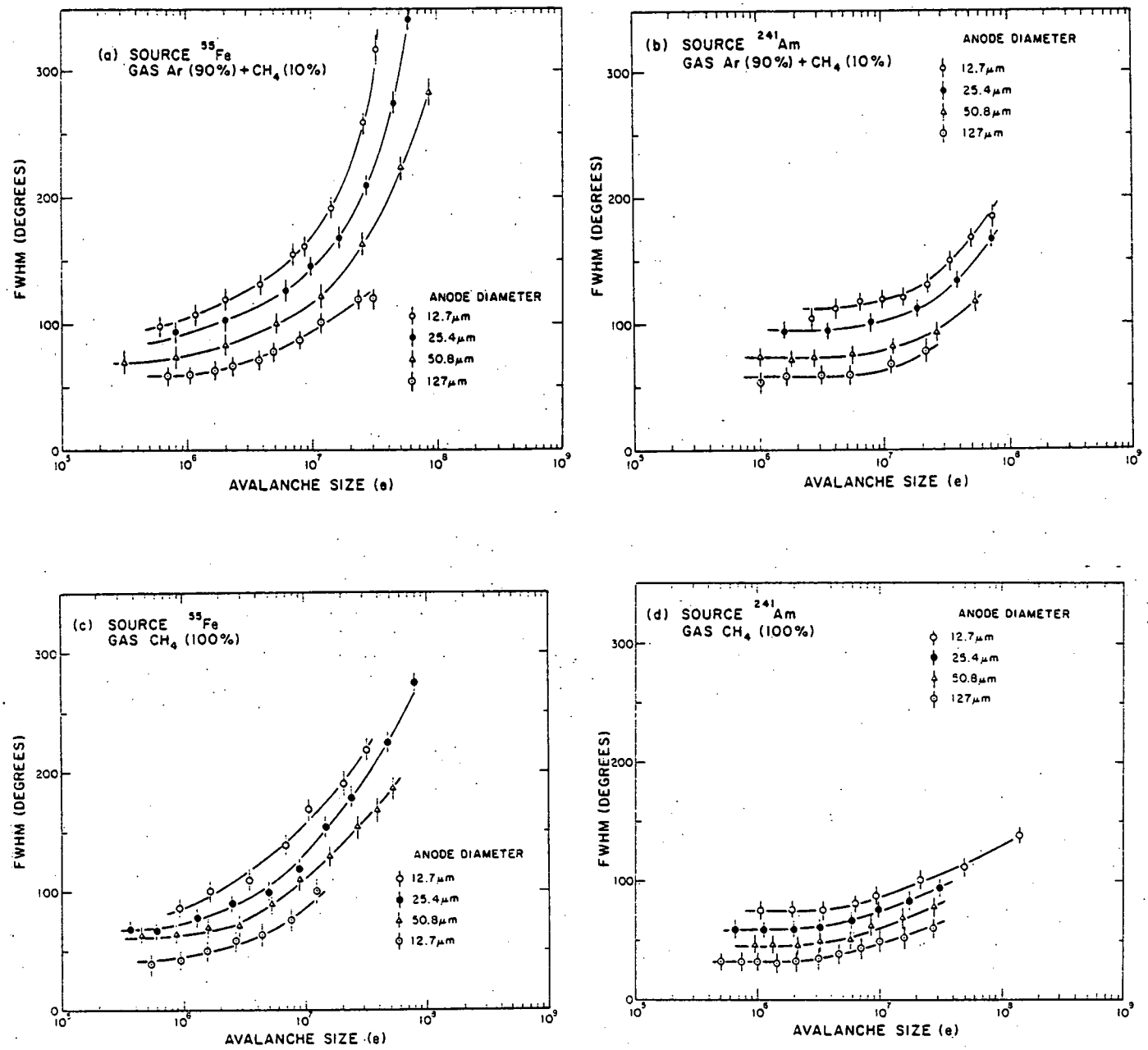

Fig. 7. FWHM of the angular distribution of the avalanche as a function of avalanche size. (a) ^{55}Fe x-rays and Ar (90%) + CH_4 (10%). (b) ^{241}Am α-rays, Ar (90%) + CH_4 (10%). (c) ^{55}Fe x-rays, CH_4 (100%). (d) ^{241}Am α-rays, CH_4 (100%).

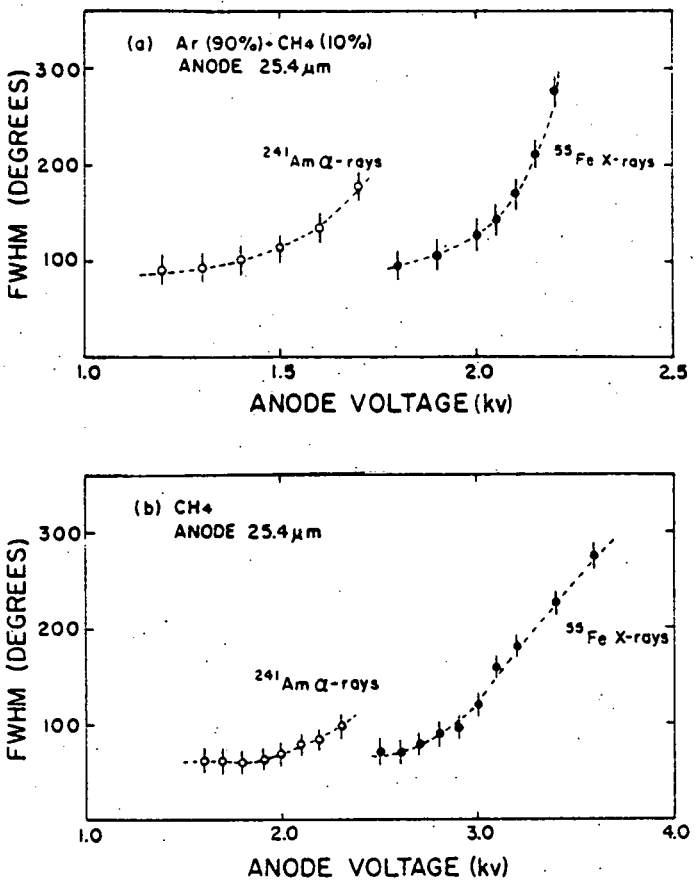

Fig. 8. FWHM of angular distribution as a function of anode voltage V_A for ^{55}Fe and ^{241}Am. (a) Ar (90%) + CH_4 (10%). (b) CH_4.

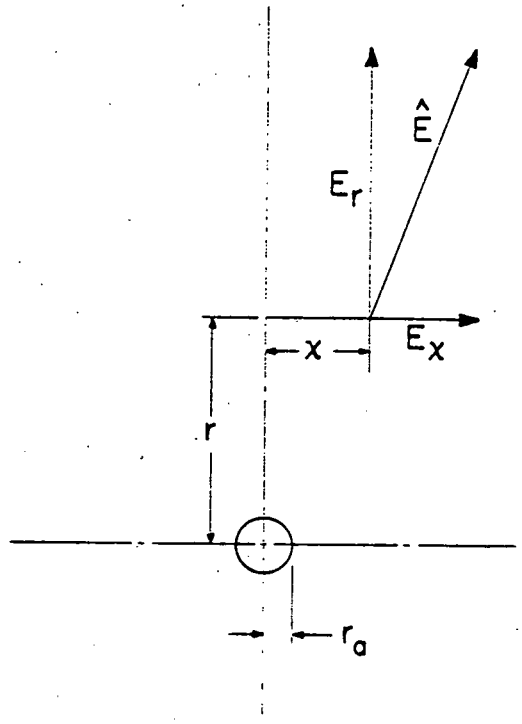

Fig. 9. Coordinates for diffusion calculation. See text.

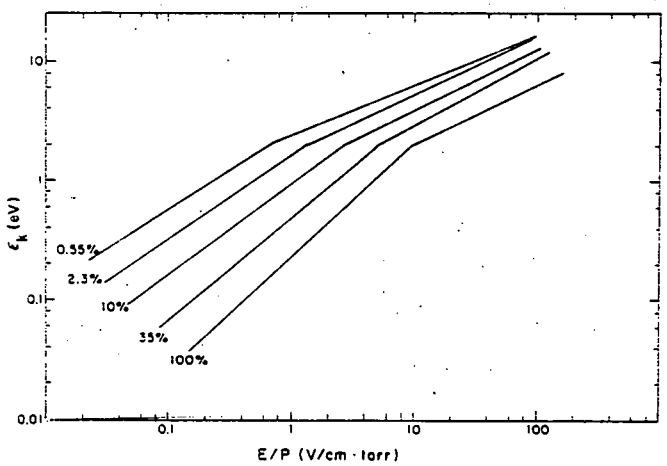

Fig. 10. Characteristic energy $\varepsilon_k = e\ D/\mu$ for Ar with various concentrations of CH_4 as a function of the reduced field strength E/p.

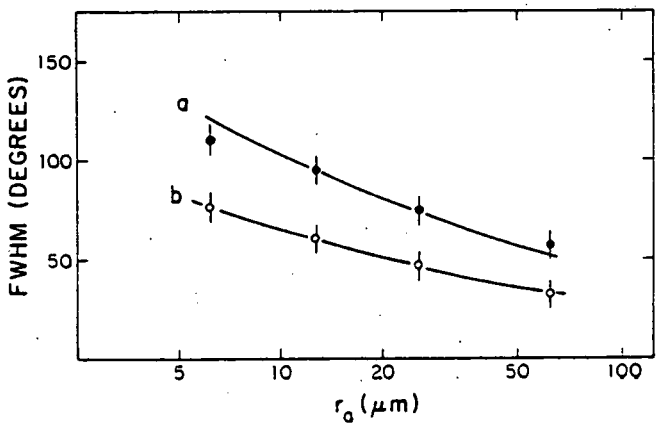

Fig. 11. FWHM of angular distribution as a function of anode radius for ^{241}Am. $Q = 2 \times 10^6 e$.

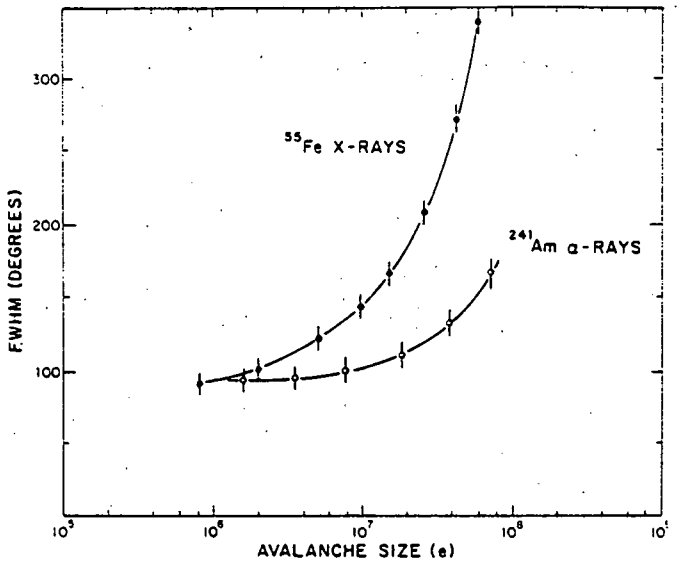

Fig. 12. FWHM of angular distribution as a function of the avalanche size Q for ^{55}Fe and ^{241}Am. Ar (90%) + CH_4 (10%).

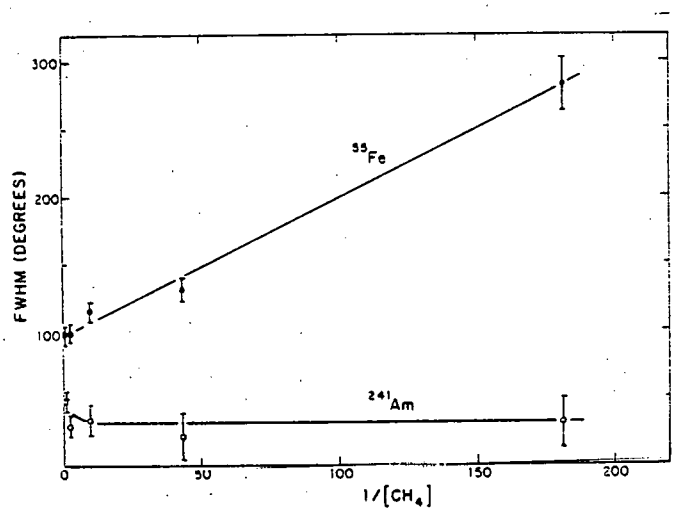

Fig. 13. FWHM of the angular distribution corrected for diffusion as a function of the inverse of the CH_4-concentration $1/[CH_4]$. Q = 2 x 10^7e, r_a = 12.7 μm.